

Computing Natural Transitions Between Tori Near Resonances in the Earth-Moon System

Stefano Bonasera*, Natasha Bosanac[†]
University of Colorado Boulder, Boulder, CO, 80303

Natural transitions between bounded motions near mean-motion resonances occur throughout our solar system and are valuable in trajectory design. Such phenomena have been examined for natural transitions between periodic orbits near resonances within multi-body systems. However, families of quasi-periodic trajectories, tracing the surface of invariant 2-tori, significantly expand the solution space of bounded motions near resonances. Yet, identifying natural transitions between spatial 2-tori has previously been cumbersome due to the high dimensionality of the associated solution space. This paper approaches the challenge in constructing these natural transfers by using a combination of Poincaré mapping, a well-known technique from dynamical systems theory, and manifold learning, a technique for dimension reduction. The presented approach involves projecting a higher-dimensional dataset of intersections recorded from the hyperbolic invariant manifolds of two 2-tori onto a lower-dimensional embedding, enabling rapid identification of initial guesses for natural transfers. These initial guesses are then corrected and input to a continuation scheme to recover families of geometrically similar transfers connecting families of invariant 2-tori. This approach is demonstrated by constructing families of natural transitions between tori near distinct resonances in the Earth-Moon circular restricted three-body problem.

I. Introduction

Natural transitions between orbits near mean-motion resonances existing in multi-body gravitational environments are of much interest in mission design and celestial mechanics. Recent missions such as the Interstellar Boundary Explorer (IBEX) and the Transiting Exoplanet Survey Satellite (TESS) missions leveraged orbits near the 3:1 and 2:1 resonances, respectively, in the Earth-Moon system [2, 3]. In these scenarios, natural motions approaching or departing a specific resonance support designing low-cost transfers or even an explanation for distinct changes in a

*Graduate Researcher, Ann and H.J. Smead Department of Aerospace Engineering Sciences, 3775 Discovery Dr., Boulder, CO, 80303, stefano.bonasera@colorado.edu.

[†]Assistant Professor, Ann and H.J. Smead Department of Aerospace Engineering Sciences, 3775 Discovery Dr., Boulder, CO, 80303, natasha.bosanac@colorado.edu.

An earlier version of this paper was presented as paper AAS 20-724 at the virtual AAS/AIAA Astrodynamics Specialist Conference in August 2020. The work in this paper also appears in the first author's Ph.D. dissertation titled "Incorporating Machine Learning into Trajectory Design Strategies in Multi-Body Systems", submitted in April 2022 to the University of Colorado Boulder. [1].

natural trajectory during long-term analyses [4-6]. In celestial mechanics, the natural transitions between orbits near mean-motion resonances offer fundamental insights into the dynamical mechanisms governing small bodies throughout the solar system; examples include the transit of comet Oterma in the Sun-Jupiter system [7-9] and the resonant sticking phenomenon of Kuiper Belt Objects (KBOs) [10].

Low-fidelity models, in combination with dynamical systems theory, provide an approximate, yet representative, framework to analyze the mechanisms governing resonance transitions in multi-body systems. For instance, the circular restricted three-body problem (CR3BP) admits a variety of dynamical structures that are approximately retained in many higher-fidelity models of multi-body systems. In the CR3BP, the set of bounded trajectories that exist near a resonance includes both periodic orbits and quasi-periodic trajectories that foliate the surface of invariant tori. Then, the intersections between stable and unstable manifolds emanating from two different periodic orbits or tori indicate the existence of natural connections, also labeled heteroclinic connections, in the CR3BP. Previous analyses of transitions between resonances in the CR3BP have tended to focus on trajectories connecting periodic orbits. For instance, Koon et al. employed Poincaré maps to investigate the transit of comet Oterma in the Sun-Jupiter system via a comparison to the planar hyperbolic invariant manifolds of orbits near resonance [7]. Haapala and Howell extended this analysis by studying three-dimensional natural motion between these resonances [11]. Building upon these works by computing and analyzing natural connections between tori near resonances is valuable for gaining a more comprehensive understanding of the wider solution space in the CR3BP. However, the stable and unstable manifolds of tori are significantly more complex than those associated with periodic orbits, producing a more challenging problem to solve from both a computation and visualization perspective.

Recent works have examined the transitions between two tori in low-fidelity models. For instance, Calleja et al. formulated a boundary value problem and numerical continuation process that enabled computation of various heteroclinic connections between periodic and quasi-periodic trajectories near L_1 and L_2 in the Earth-Moon CR3BP [12]. Another approach developed by Jorba, Gómez and Mondelo, and Olikara and Scheeres enables efficient numerical computation of invariant tori and their invariant hyperbolic manifolds [13-15]. With these tools, Olikara has used two approaches to construct natural transfers between two invariant tori near libration points in the CR3BP. In the first approach, connections were computed from a fixed departure torus to an a posteriori defined arrival torus using arcs that remain bounded within a specified neighborhood of the smaller primary; in the second approach, Olikara recovered a connection between two spatial quasi-periodic trajectories via continuation from a natural transfer between two nearby planar orbits [16]. Using these tools as a foundation, McCarthy also computed natural and maneuver-enabled transfers between quasi-periodic trajectories near L_1 and L_2 in both the Earth-Moon CR3BP and an ephemeris model [17]. In addition, Kumar et al. have used Graphical Processing Units to identify the intersections of stable and unstable manifolds of tori near resonances in periodically perturbed systems to recover heteroclinic connections [18].

To study the natural transitions between spatial invariant tori near resonances, this paper leverages a combination

of traditional dynamical systems and unsupervised learning techniques. A primary challenge in constructing spatial transfers between periodic solutions in the CR3BP is that a Poincaré map capturing the arcs used to construct an initial guess is high-dimensional. Computing natural transfers between spatial invariant tori increases the inherent challenge of the problem, due to the larger dimensionality of the solution space. To visualize the hyperbolic invariant manifolds associated with invariant tori via Poincaré mapping, a technique from manifold learning is employed in this paper. Manifold learning is a nonlinear dimension reduction method that focuses on discovering a lower-dimensional manifold that a higher-dimensional dataset is assumed to lie on, thereby reducing the complexity of visualizing and analyzing the dataset [19]. In our paper, the high-dimensional state information encoded in each map crossing is projected onto a lower-dimensional embedding that is calculated via Uniform Manifold Approximation and Projection (UMAP) [20]. This state-of-the-art technique minimizes the topological distance between the high- and low-dimensional spaces [20]. Due to this theoretical foundation, UMAP has been used to analyze a wide variety of complex datasets and, therefore, investigate phenomena in the associated nonlinear systems including complex proteins in single cell biology [21], genetic structures in cohorts [22], and the origin of solar wind [23]. UMAP is used in this paper to aid in the visualization of the high-dimensional crossings on a Poincaré map, aiding the trajectory designer in identifying initial guesses for natural transfers between distinct 2-tori.

This paper focuses on constructing families of natural transfers between invariant 2-tori in the Earth-Moon CR3BP, using techniques from dynamical systems theory and manifold learning. This procedure is demonstrated in the context of natural transitions from tori near the 3:2 resonance to tori near the 1:2 resonance, but may be used to compute natural transfers between various other unstable 2-tori. First, families of spatial quasi-periodic trajectories near two selected resonances are computed. Then, the hyperbolic invariant manifolds associated with two members of these families of invariant tori are calculated and represented by their intersections with a surface of section. The resulting higher-dimensional crossings of the Poincaré map are projected and visualized onto a two-dimensional embedding that is constructed via UMAP. Then, two crossings from each manifold structure, that are located nearby in the lower-dimensional space, are used to seed an initial guess for the natural transfer. Because UMAP generates a low-dimensional embedding with a topological structure that balances approximating the global and local characteristics of the original higher-dimensional space, the selected two crossings in the low-dimensional representation are likely to be located nearby in the original higher-dimensional phase space. Thus, the reduced representation of a higher-dimensional Poincaré map via UMAP offers a useful visualization that supports rapid identification of candidate arcs that resemble natural connections. Then, the selected discontinuous arcs are refined numerically to produce a continuous solution. Finally, continuation is used to compute a family of geometrically similar natural transfers between other members of the same families of invariant tori. These natural transfer sets supply preliminary insights into the existence and geometric properties of natural transitions between invariant tori near the two selected resonances in multi-body systems. Transfers are also constructed from tori near the 1:3 to tori near the 3:1 resonances and from tori near the 2:3 to tori near

the 1:5 resonance to demonstrate the applicability of the presented approach to other types of natural transitions.

II. Dynamical Model

This paper uses the CR3BP to approximate the motion of an object due to the gravitational influence of two primary bodies. In the CR3BP, two point mass primaries, P_1 and P_2 , are assumed to follow circular orbits about their mutual barycenter. The third body, P_3 , representing a spacecraft or a small body, is assumed to possess a negligible mass with respect to P_1 and P_2 [24]. Then, mass, length and time parameters are nondimensionalized. Consequently, a mass parameter μ represents the ratio between the mass of the smallest primary and the total mass of the system: in the Earth-Moon system, $\mu \approx 0.01215$. In addition, a rotating orthogonal reference frame is defined with an origin at the system barycenter and the axes $(\hat{x}, \hat{y}, \hat{z})$: \hat{x} is directed from P_1 to P_2 , \hat{z} is parallel to the orbital angular momentum vector of the primaries, while \hat{y} completes the right-handed triad. The nondimensional state of P_3 is defined in the rotating frame as $s = [x, y, z, \dot{x}, \dot{y}, \dot{z}]^T$. Then, the nondimensional equations of motion in the CR3BP for P_3 are written as:

$$\ddot{x} - 2\dot{y} = U_x, \quad \ddot{y} + 2\dot{x} = U_y, \quad \ddot{z} = U_z \quad (1)$$

where the pseudo-potential function is $U(s) = (x^2 + y^2)/2 + (1 - \mu)/r_1 + \mu/r_2$ and U_x, U_y and U_z denote the partial derivatives of U with respect to x, y and z , respectively. The distances of P_3 from the two primaries are $r_1 = \sqrt{(x + \mu)^2 + y^2 + z^2}$ and $r_2 = \sqrt{(x - 1 + \mu)^2 + y^2 + z^2}$. In this system, the Jacobi constant, an integral of motion, is defined as $C_J(s) = 2U(s) - \dot{x}^2 - \dot{y}^2 - \dot{z}^2$ [24]. At a fixed value of C_J , a wide variety of fundamental solutions exist, including: five Lagrange points, labeled L_i for $i = \{1, \dots, 5\}$; periodic orbits; and quasi-periodic trajectories.

III. Periodic Orbits near Mean-Motion Resonances

The definition of a mean-motion orbital resonance is inherited from Keplerian dynamics, where two assumed massless particles, B and C, are subject to the gravitational influence of a single point-mass central body, A. Particle B is in resonant motion with C if B completes exactly p orbits about A in the same time C revolves q times around A, with $p, q, \in \mathbb{N}^+$ [25] [26]. The $p : q$ resonance is classified as interior when $p > q$ or exterior when $p < q$ [26]. When this definition is transitioned to the CR3BP, the body B is the assumed massless P_3 whereas body A is P_1 and body C is P_2 , e.g. the Earth and the Moon, respectively. In this paper, an initial guess for a planar $p : q$ resonant periodic orbit is constructed in the two-body problem, following the procedure presented by Vaquero and Anderson [25] [26]. The initial guess is then transformed into the rotating coordinate system. Next, differential correction is used to recover a nearby periodic orbit in the CR3BP. Using this single periodic orbit, pseudo arc-length continuation is used to generate additional members of the same family. Although typically labeled a $p : q$ resonant orbit family, only a finite number of members may possess a period that is exactly resonant with the primary system; additional orbits along the family

possess a period that evolves away from the resonance [25-27].

The stability characteristics of a periodic orbit are used to gain insight into the nearby flow. A periodic orbit is uniquely defined in the CR3BP by a state $s(t) \in \mathbb{R}^6$ and orbital period T . Then, the state transition matrix (STM) $\Phi(t, t_0)$ supplies a linear mapping between a deviation from the initial state $\delta s(t_0)$, to a deviation from a subsequent state $\delta s(t) = \Phi(t, t_0)\delta s(t_0)$. The monodromy matrix is then defined as the STM evaluated over an orbital period, i.e., $M = \Phi(t_0 + T, t_0)$. Spectral decomposition of the monodromy matrix produces six eigenvalues in reciprocal or complex conjugate pairs and associated eigenvectors [28]. For planar periodic orbits, two nontrivial eigenvalue pairs reflect the characteristics of nearby in-plane and out-of-plane motion: an eigenvalue with a magnitude larger than unity is associated with an unstable mode; an eigenvalue with magnitude lower than unity identifies a stable mode; and a complex conjugate pair of eigenvalues with unitary magnitude is associated with nearby oscillatory motion [24].

Two fundamental motions emerge when a periodic orbit is perturbed along one of the nontrivial eigenvalues. When a single state along the orbit is perturbed along the locally stable (unstable) mode, the perturbed state produces a trajectory that naturally approaches the periodic orbit as $t \rightarrow +\infty$ ($t \rightarrow -\infty$). The collection of all the trajectories exhibiting this characteristic is labeled the stable (unstable) invariant manifold. Heteroclinic transfers between two distinct periodic orbits exist when their stable and unstable invariant manifolds intersect: these arcs correspond to a natural transfer between two periodic orbits in infinite time. Quasi-periodic trajectories, however, lie within the center manifold of a periodic orbit with oscillatory modes [29].

IV. Quasi-Periodic Trajectories and Invariant 2-Tori

A quasi-periodic trajectory is a bounded path that traces out the surface of an invariant torus; this paper focuses specifically on spatial 2-tori governed by two fundamental frequencies. A state on the surface of a 2-torus may be described by two angular quantities $[\theta_1(t), \theta_2(t)]$, associated with the longitudinal and transverse directions, respectively. The associated fundamental frequencies, ω_1 and ω_2 , of a bounded quasi-periodic trajectory are incommensurate. This paper uses the approach developed by Jorba, Gómez and Mondelo, and Olikara and Scheeres to compute a torus traced out by a quasi-periodic trajectory in the CR3BP [13-15]. In this approach, a torus is computed by recovering an invariant curve that is defined as follows: a state $s(\theta_1, \theta_2)$ that begins on the invariant curve returns to the curve when propagated forward in time for a stroboscopic mapping time $T = 2\pi/\omega_1$ and undergoes a rotation on the curve by an angle $\rho = 2\pi\omega_2/\omega_1$. This invariant curve satisfies the following invariance condition:

$$R_{-\rho}\varphi_T(s(\theta_1, \theta_2)) - s(\theta_1, \theta_2) = \mathbf{0} \quad (2)$$

where $R_{-\rho}$ is a rotational operator and $\varphi_T(s(\theta_1, \theta_2))$ corresponds to the first return to a stroboscopic map with time T for the state $s(\theta_1, \theta_2)$. To reduce computational complexity, the invariant curve is approximated via a truncated Fourier

series calculated using an odd number of N_Q states, equally spaced in θ_2 . As a result, the operator $R_{-\rho}$ is transformed into a combined sequence of matrices, $\mathbf{R}(-\rho)$. By aggregating the points sampled along the invariant curve into a matrix as $\mathbf{U} \in \mathbf{R}^{N_Q \times 6}$, a numerical approximation of the invariance condition is:

$$\mathbf{S} = \text{vec}(\mathbf{R}(-\rho)\varphi_T(\mathbf{U}(\theta_1, \theta_2)) - \mathbf{U}(\theta_1, \theta_2)) = \mathbf{0} \in \mathbf{R}^{6N_Q} \quad (3)$$

where the condition is vectorized by the $\text{vec}(\cdot)$ operator. To compute a torus that lies close to a periodic orbit with oscillatory modes, a state s_0 along the periodic orbit is defined, corresponding to a longitudinal angle $\theta_1 = 0$. The eigenvector \mathbf{v}_C , associated with the complex unitary eigenvalue λ_C of \mathbf{M} is used to compute N_Q states along an initial guess for an invariant curve as:

$$s(\theta_1, \theta_{2,i}) = s_0 + \epsilon(\text{Re}[\mathbf{v}_C] \cos \theta_{2,i} + \text{Im}[\mathbf{v}_C] \sin \theta_{2,i}) \quad (4)$$

where an odd number of equally spaced values of the transverse toroidal angle θ_2 are used and ϵ is a small scalar value. To construct the initial guess, the period of the underlying periodic orbit is used as an approximation for the stroboscopic mapping time T , while the rotation angle is approximated as $\rho = \text{Re}[-i \ln \lambda_C]$.

The constructed initial guess is corrected via multiple shooting [30]. First, the N_Q states that have been sampled along an initial guess for an invariant curve are each propagated forward in time and their trajectories sampled to produce an initial guess for M_Q subsequent invariant curves that are located at equally-spaced time intervals along the torus in the longitudinal direction. These $N_Q(M_Q + 1)$ states, as well as T and ρ , are simultaneously corrected until the following constraints are satisfied to within a specified tolerance: 1) when the first M_Q invariant curves are propagated forward in time for $T/(M_Q + 1)$, they satisfy full state continuity with the subsequent invariant curves; and 2) the invariance condition is satisfied by the states generated by propagating the final invariant curve forward in time for $T/(M_Q + 1)$. Additional constraints are often applied to the Jacobi constant and other parameters [16]. In this paper, a one-parameter family of invariant tori is computed at a single energy level by constraining the average Jacobi constant for the states along the initial invariant curve. Once a single torus has been computed, pseudo-arclength continuation is employed to recover additional members of the family of invariant 2-tori. Consistent with other numerical procedures that are commonly used to compute fundamental solutions in the CR3BP, each torus within this family is not exactly recovered by this approach due to the approximation introduced by the discrete Fourier transform, the use of numerical integration, and the nonzero tolerance used to assess whether the constraint vector is satisfied. However, the resulting numerical solutions tend to lie sufficiently close to tori that exist at a single value of the Jacobi constant [31].

Once an invariant torus has been computed, the nearby linearized dynamical flow supplies useful information on the associated stability. Specifically, the stability of a torus is evaluated by inspecting the eigenstructure of the differential of

the invariance condition, labeled DS . Following the work of Jorba, the eigenvalues of DS correspond to concentric circles about the origin in the Gauss plane [13]. Each of these circles is associated with a radius R in the complex plane. Analogous to the stability of periodic orbits, if non-unitary radii exist, the torus possesses stable and unstable modes [13] [17]. After perturbing the approximated invariant curve along the locally stable (unstable) mode, the perturbed states naturally approach the torus for $t \rightarrow +\infty$ ($t \rightarrow -\infty$) [16]. The collection of all the states naturally approaching (departing) the underlying torus in forward time lies on the stable (unstable) invariant manifold of the torus. This paper focuses on computing natural connections between invariant 2-tori near resonant orbit families and using the associated stable and unstable manifolds to construct an initial guess.

V. Using Dimension Reduction to Visualize Higher-Dimensional Poincaré Maps

A. Poincaré Maps

In dynamical systems theory, Poincaré maps reduce the complexity of visualizing a large set of trajectories by transforming a continuous solution into a sequence of discrete states. The first step in constructing a Poincaré map is defining a surface of section that is transverse to the flow of interest [29]. There are a variety of useful definitions of a surface of section to capture the flow in the CR3BP: events such as the minimum or maximum distance from a central body (i.e., apsides); functions of state coordinates; and stroboscopic maps that capture the flow at specific constant times [29]. Once a surface of section has been defined, trajectories are propagated, either forward or backward in time, from a specified set of initial conditions. The intersections of these generated arcs with the surface of section are recorded and visualized in a lower-dimensional space via a Poincaré map [32].

Poincaré maps have been used extensively to construct initial guesses for heteroclinic connections between planar periodic orbits. Following a similar methodology to Koon et al., consider two planar periodic orbits near the resonances of interest in this paper, as displayed in Fig. 1a). This figure displays periodic orbits in the interior 3:2 (magenta) and exterior 1:2 (blue) resonant orbit families in the Earth-Moon CR3BP at the same Jacobi constant of $C_J = 2.73$. The Earth and Moon are indicated using gray circles, while the equilibrium points are indicated by red diamonds. A stability analysis reveals that these two periodic orbits each admit stable and unstable manifolds. To visualize these manifolds, a surface of section is defined at $y = 0$. Trajectories along the unstable manifold associated with the 3:2 resonant orbit and the stable manifold associated with the 1:2 resonance are propagated, with up to 10 intersections with the surface of section recorded when $\dot{y} > 0$. Figure 1b) displays these intersections of the unstable manifold of the 3:2 orbit (magenta) and the stable manifold for the 1:2 resonant orbit (blue) on a one-sided Poincaré map where each crossing is visualized in the (x, \dot{x}) plane. Each map crossing in this example is uniquely represented in this two-dimensional plot. Thus, intersections between the curves formed by each of the blue and magenta colored crossings indicates the existence of a natural transfer from the 3:2 orbit to the 1:2 resonant orbit. This natural transfer is computed by first locating two nearby

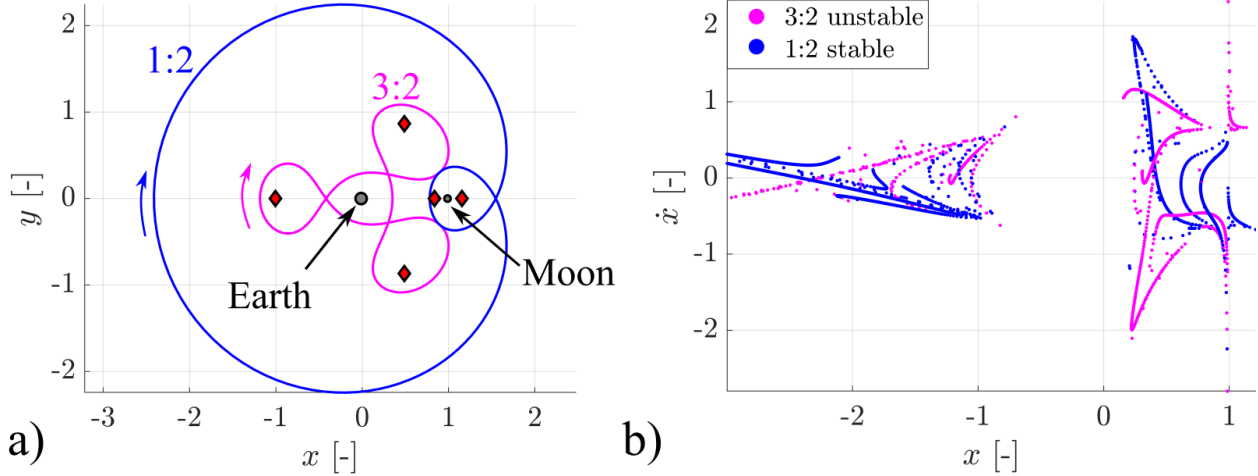


Fig. 1 Periodic orbits at $C_J = 2.73$ near the a) 1:2 (blue) and 3:2 (magenta) resonances, with Lagrange points (red), and b) associated hyperbolic manifold crossings.

crossings of the map – one from each hyperbolic invariant manifold – and using them to construct an initial guess. This initial guess is then corrected to produce a continuous trajectory. The resulting trajectories are interchangeably referred to as heteroclinic connections, natural transfers, and natural transitions throughout this paper. Of course, this type of trajectory is an approximation to a nearby heteroclinic connection between the two periodic orbits due to the use of numerical methods.

When the trajectories of interest are spatial, the associated Poincaré map may appear as a dense set of higher-dimensional crossings that are challenging to analyze via a two- or three-dimensional projection. Researchers in the astrodynamics community have introduced strategies to address some of these challenges. For instance, Gomez et al. constructed an initial guess for a spatial heteroclinic connection between two orbits in the CR3BP by locating the intersections of their stable and unstable manifolds on a four-dimensional Poincaré map. To achieve this goal, they applied additional constraints to the map crossings to examine a smaller subset of the data via a bijective, two-dimensional map [33]. Alternatively, Haapala and Howell constructed heteroclinic connections between spatial libration point orbits to examine the dynamical mechanisms that govern cometary transits in the Sun-Jupiter systems. To construct initial guesses for these transfers using stable and unstable manifolds of periodic and quasi-periodic trajectories, they used glyphs, a graphical object that produces a visual representation of multivariate data. Through this approach, they constructed initial guesses for natural transfers from arcs with nearby map crossings that possess similar glyphs. In these examples, these approaches to Poincaré map visualization have created a valuable foundation for examining natural transport mechanisms and trajectory design in multi-body systems [11]. In this paper, however, an alternative approach to visualization of higher-dimensional Poincaré maps is presented to accommodate increasingly complex scenarios, while avoiding data obscuration, over-constraining the solution space, and a high workload for the human analyst. Specifically, a manifold learning technique is used to project higher-dimensional data associated with Poincaré

map crossings onto a lower-dimensional embedding, reducing the complexity of analysis.

B. Manifold learning

Manifold learning techniques, such as the Uniform Manifold Approximation and Projection (UMAP), are a form of dimension reduction algorithms. Dimension reduction is founded in the premise that the descriptions used to form high-dimensional dataset may contain redundant information but may be adequately described by only a key set of latent features [20, 34]. UMAP approaches this problem by constructing a low-dimensional representation of a nonlinear dataset to minimize the topological distance between the manifolds associated with the high- and low-dimensional descriptions. To implement this process, concepts from algebraic and fuzzy topology are leveraged. First, the algorithm assumes that the high-dimensional dataset is uniformly distributed on a manifold; UMAP seeks to infer the Riemannian metric on the manifold that would result in such a distribution. Under the assumption of a locally connected manifold, UMAP leverages fuzzy simplicial sets to construct these local metrics and define a weighted graph that captures the fuzzy topological structure of the high-dimensional dataset. Then, the algorithm leverages optimization to minimize the difference between the topological representations of the low-dimensional description and the high-dimensional dataset. UMAP initializes the lower-dimensional projection with spectral embedding techniques and then refines it by minimizing the cross entropy between the 1-simplices of the high- and low-dimensional representations. This optimization step leverages stochastic gradient descent for computational efficiency. However, to support reproducibility of the results, the random state may be fixed at the expense of a minor increase in computational time. This algorithm is accessed in this paper via the *umap-learn* library available in Python [20, 34].

To apply UMAP to a particular dataset, several input parameters must be selected; the exact combination of selected parameters impacts the characteristics of the dataset projected onto the constructed lower-dimensional embedding. The three most significant input parameters include n_n , m_{dist} and n_c : $n_n \in \mathbb{N}^+$ influences the number of neighbors used when constructing the local fuzzy simplicial sets that form the basis for the graph representation of the high-dimensional dataset, thereby balancing capturing the local versus global structure in the dataset with low values producing an embedding that prioritizes the local manifold structure; $m_{dist} \in [0, 1]$ is the minimum separation between two nearby points in the lower-dimensional space, thereby balancing the density level of the embeddings, ranging from low values and highly dense solutions to large values and sparse embeddings; and $n_c \in \mathbb{N}^+$ defines the dimension of the lower-dimensional Euclidean representation [20]. In this paper, large values of n_n and low values for m_{dist} are selected manually via an iterative approach: this parameterization prioritizes a compact visualization of the overall global structure, while also minimizing the effects of data obscuration. Moreover, the obtained datasets are projected into a two-dimensional Euclidean space with $n_c = 2$ selected to simplify visualization. The overall computational complexity of UMAP when applied to a dataset composed of N members is driven by the graph, empirically approximated as $\sim O(N^{1.14})$, and the stochastic gradient descent step, $\sim O(n_n N)$ [20].

VI. Computing Natural Transitions Between Spatial Invariant 2-Tori

This paper uses Poincaré mapping, manifold learning, and constrained optimization to construct natural transitions between invariant 2-tori near distinct resonances. The approach consists of two fundamental phases. The first phase focuses on constructing a discontinuous initial guess for a natural connection between two spatial invariant tori. This phase begins by computing two families of tori near distinct resonances and at a constrained value of the Jacobi constant. The crossings of the hyperbolic manifolds associated with two selected members of these families with a common surface of section are used to generate a higher-dimensional Poincaré map. Then, UMAP is used to project the higher-dimensional crossings onto a lower-dimensional representation. Using this alternative representation mitigates the impact of data obscuration often encountered when visualizing high-dimensional Poincaré maps and enables a rapid identification of initial guesses for a heteroclinic connection from nearby projected map crossings of the two manifold structures without imposing further constraints on the solution space. In the second phase, the initial guess is numerically corrected to produce a continuous natural transfer between the two selected invariant tori. Continuation is then used to compute similar natural transitions between other members of each family of spatial 2-tori near resonances.

A. Initial Guess Generation

Poincaré mapping and manifold learning are leveraged, in combination, to construct an initial guess for a natural transition between spatial invariant tori near distinct resonances. The process is summarized as follows:

- 1) *Compute each family of invariant 2-tori:* Two planar orbits near distinct resonances at the same value of Jacobi constant C_J are selected. The selected orbits possess both hyperbolic and center manifolds to ensure that a nearby family of invariant 2-tori exists and, through inheriting the stability of the periodic orbit, admit trajectories that naturally depart and approach the torus. The numerical approach presented by Jorba, Gómez and Mondelo, and Olikara and Scheeres is used to calculate these two families of tori, enforcing a fixed value of the average Jacobi constant for the initial invariant curve [13-15]. This step produces two families of unstable tori that are all described by the same average value of the Jacobi constant, evaluated using the states along each of the computed invariant curves. To generate each trajectory, a Runge-Kutta Prince-Dormand (8, 9) integration scheme is implemented in C++ using the GNU Scientific Library with an absolute tolerance of 10^{-15} and relative tolerance of 10^{-14} [35].
- 2) *Define the surface of section:* A surface of section is first defined to capture the flow associated with the hyperbolic invariant manifolds of the selected invariant tori. In this work, a surface of section with $y = 0$ is employed with no additional constraints on the sign of the velocity components at each crossing, thereby producing a two-sided Poincaré map.
- 3) *Record crossings of the manifolds on the Poincaré map:* One invariant torus is selected from each family to possess similar maximum out-of-plane components; tori with this property are empirically observed to offer a

good starting point for locating the first heteroclinic connection. The stable and unstable manifolds associated with each of the selected tori are generated using a small displacement, equivalent to 100 km in the configuration space, along the stable and unstable eigenvectors, respectively. Then, for the primary example presented in this paper, up to 12 crossings with the surface of section are recorded. However, the hyperbolic invariant manifolds associated with these two tori and generated with the specified step size tend to remain in their vicinity for approximately 6 revolutions. The associated first 6 crossings are generally not useful for locating intersections of the stable and unstable manifolds of the investigated tori. Thus, only the 7th to 12th crossing of the manifolds with the surface of section are analyzed.

- 4) *Construct a lower-dimensional projection via UMAP:* The map crossings associated with the hyperbolic invariant manifolds form a five-dimensional dataset: each map crossing is described by the phase space variables $[x, z, \dot{x}, \dot{y}, \dot{z}]$. The dimension of the dataset is not reduced any further because distinct invariant curves are computed using the procedure outlined in Sec. [IV](#) to possess only the same average value of the Jacobi constant over N_Q states. Thus, the map crossings of the trajectories generated to approximate the stable and unstable manifolds of the tori may exhibit small deviations in the Jacobi constant across the dataset. UMAP is then used to project the five-dimensional data onto a two-dimensional Euclidean space: the dimension of the embedding is selected to prevent data obscuration in representations with more than two dimensions, and is consistent with the dimension of states along the surface of a torus, identified by two angular quantities, $[\theta_1(t), \theta_2(t)]$. The input parameters governing UMAP are also selected as $n_n = 100$ and $m_{dist} = 0.0$ to supply a compact representation that focuses on retaining the global structure of the map crossings.
- 5) *Construct an initial guess:* An intersection between a stable and unstable manifold arc in the five-dimensional phase space indicates the existence of a natural transition between the two tori. Because UMAP seeks to minimize the difference between the topological representations of the low-dimensional description and the high-dimensional dataset, areas where the projected map crossings possess low relative distances on the two-dimensional embedding are investigated as candidate regions for locating connections between the stable and unstable manifolds in the full phase space. In these areas, two crossings (one from each of the stable and unstable manifolds) that lie nearby in the lower-dimensional representation are selected to produce arcs that form an initial guess for a heteroclinic connection between two tori. Next, the selected map crossings are propagated backward and forward in time to generate the associated unstable and stable manifold arcs, respectively. Three revolutions of the associated tori are concatenated to the beginning and end of the transfer to form a suitable initial guess.

The presented procedure, used for initial guess generation, is demonstrated in this paper by constructing a transfer between spatial invariant tori near distinct resonances in the Earth-Moon CR3BP. However, the presented technique may be applied to identify existing natural connections between other pairs of unstable invariant tori.

B. Trajectory correction and continuation

The constructed initial guess is used to recover a family of continuous and natural transfers between spatial invariant tori near two distinct resonances. The correction scheme is designed to both enforce continuity between each hyperbolic invariant manifold arc and ensure the trajectory flows away from or into each of the selected tori. In this paper, a multiple shooting algorithm is formulated as an optimization problem that is implemented using Matlab's *fmincon* function [36]. The objective function is designed to minimize the discontinuity between each torus and the initial and final states along the transfer; along with equality constraints that enforce continuity, solutions that minimize this objective below a specified threshold are deemed to sufficiently reflect a nearby natural connection. Of course, this procedure is conceptually equivalent to implementing a multiple shooting algorithm using only equality constraints. However, formulating this problem as an optimization problem was observed to produce a less numerically sensitive process. Mitigation of the sensitivities observed in a traditional equality constraint formulation is an ongoing effort to be addressed in future work. Nevertheless, the presented approach supplies solutions that correspond to natural transitions between two tori, to within a selected numerical tolerance.

To define the optimization problem for implementing corrections, free variable and constraint vectors are defined, along with the objective function. First, the initial guess is discretized into $M-1$ arcs. To completely describe these arcs, the free variable vector is defined as:

$$\mathbf{V} = [s_1, s_2, \dots, s_M, t_{1,2}, t_{2,3}, \dots, t_{M-1,M}]^T \in \mathbb{R}^{7M-1} \quad (5)$$

with s_i for $i \in [1, M]$ representing the states at the beginning of each arc and end of the last arc and $t_{j,j+1}$ denoting the propagation time from the beginning of arc j to the end of the arc. Each trajectory, described by \mathbf{V} , must be continuous. Full state continuity is enforced using the following constraint vector:

$$\mathbf{F}(\mathbf{V}) = [s_1(t_{1,2}) - s_2, s_2(t_{2,3}) - s_3, \dots, s_{M-1}(t_{M-1,M}) - s_M]^T \in \mathbb{R}^{6(M-1)} \quad (6)$$

where $s_i(t_{i,i+1})$ is the state at the end of the i th arc. Then, the optimization problem is stated as:

$$\mathbf{V} = \arg \min_{\mathbf{V}} f(\mathbf{V}) \quad \text{subject to} \quad \mathbf{F}(\mathbf{V}) = \mathbf{0} \quad (7)$$

for a scalar objective function $f(\mathbf{V})$. In this paper, the objective function is designed to ensure minimization of the discontinuity between the initial and terminal states along the transfer and the associated tori; conceptually, this corresponds to the requirement that the beginning of the transfer naturally flows away from the initial torus and the end

of the transfer naturally flows into the final torus. Mathematically, this objective function is written as:

$$f(\mathbf{V}) = \|s_1 - s_{T1}\|^2 + \|s_M - s_{T2}\|^2 \quad (8)$$

where s_{T1} and s_{T2} are the closest states along each torus to the initial and final states s_1 and s_M along the transfer.

The states s_{T1} and s_{T2} are computed at each iteration of the optimization scheme from the set of approximate invariant curves along the departure and arrival tori. To compute s_{T1} and evaluate the first term of the cost function, the closest invariant curve $U(\theta_1, \theta_2)$ on the departure torus to s_1 at the beginning of the transfer is located. A single shooting approach is used to obtain the closest point on the torus to s_1 , i.e. s_{T1} . Specifically, the invariant curve $U(\theta_1, \theta_2)$ is rotated in the longitudinal direction by an angle τ_1 to produce the invariant curve $U(\theta_1 + \tau_1, \theta_2)$: this rotation corresponds to forward propagation of the states sampled from $U(\theta_1, \theta_2)$. Then, the curve $U(\theta_1 + \tau_1, \theta_2)$ is rotated in the transverse direction by an angle τ_2 , using the rotation operator $\mathbf{R}(\cdot)$. Therefore, this scheme uses a free variable vector $\mathbf{Y} = [\tau_1, \tau_2] \in \mathbb{R}^2$. Then, the first state along this invariant curve is iteratively adjusted to approach s_1 . Specifically, \mathbf{Y} is updated 10 times by taking steps in the Newton direction, calculated using the following vector:

$$\mathbf{G}(\mathbf{Y}) = s_1 - \mathbf{R}(\tau_2)U(\theta_1 + \tau_1, \theta_2)|_1 \quad (9)$$

While $\mathbf{G}(\mathbf{Y})$ cannot equal zero, because a state cannot simultaneously lie along a natural transfer and a torus, this approach produces a free variable vector \mathbf{Y} that results in a small magnitude for $\mathbf{G}(\mathbf{Y})$, indicating the recovery of a nearby state along the torus. This method is successful with a general initial guess $\mathbf{Y} = (0.01, 0.01)$ if the torus is originally described by a sufficiently large number of invariant curves. A similar procedure is used to evaluate the second term in the objective function using the arrival torus.

The formulated optimization problem is solved using interior point optimization in the MATLAB routine *fmincon* [36]. Because both tori are constrained to possess the same average Jacobi constant, a transfer is considered a natural connection if it corresponds to an objective $f(\mathbf{V}) \leq 10^{-12}$ and a constraint vector magnitude $\|\mathbf{F}(\mathbf{V})\|_2 \leq 10^{-12}$. The threshold in the objective function corresponds to a cumulative approximate displacement of 400 m and 1 mm/s in the Earth-Moon system from the departure and arrival torus. This value is reasonable given the nonzero difference between the minimum and maximum Jacobi constants of states along each invariant curve, which is a direct consequence of using a truncated Fourier series representation of the curve to numerically generate an approximation to an invariant torus.

Once the optimization strategy recovers a transfer between the two selected tori, a continuation scheme is used to generate geometrically similar transfers between other members of the two families of invariant tori. This continuation approach follows a grid-like structure: initially, the departure torus is fixed, while the arrival torus is gradually adjusted to step along the family. At each step of this continuation process, the transfer connecting one combination of tori is

used to seed the initial guess for the next combination of tori. This process terminates when there are either no more members along the arrival torus family or a feasible transfer cannot be computed. Then, a similar procedure is repeated for each new departure torus. This procedure enables computation of a natural connection, with a similar geometry to the initial guess, between spatial tori along the two selected families. Note that the continuation scheme presented in this paper only seeks the existence of one transfer between each combination of tori and within the neighborhood of the initial guess. Similar solutions may also be generated by varying the departure and arrival locations along each torus. Such an analysis may also, potentially, expand the combinations of arrival and departure tori that admit a natural connection. Nevertheless, the implemented approach enables a preliminary analysis of natural transitions between bounded motions near resonances.

VII. Natural Transitions Between Tori Near Distinct Resonances

Natural transfers between invariant 2-tori near the 3:2 and 1:2 resonances in the Earth-Moon CR3BP are constructed and analyzed. First, point solutions are rapidly recovered using Poincaré mapping, manifold learning, and corrections. Then, a specific region of the Poincaré map is analyzed in the lower-dimensional space constructed by UMAP to construct multiple transfers and their geometries compared. Two natural transfers are then used in a continuation scheme to recover geometrically similar arcs connecting other members of the two families of invariant tori.

A. Recovering Point Solutions for Natural Transfers

Families of invariant tori near the 3:2 and 1:2 resonances are generated in the Earth-Moon CR3BP. First, consider the two planar periodic orbits, one from each family, that are depicted in the center of Fig. 2. In this figure, the Earth and the Moon are displayed as gray circles, and the Lagrange points are denoted with magenta diamonds. These planar periodic orbits exist at a Jacobi constant of $C_J = 2.73$ with approximate periods of 55.92 days and 50.54 days, respectively. At this energy level, periodic orbits in both families admit planar hyperbolic invariant manifolds and a spatial center manifold. Families of nearby invariant 2-tori are then generated at this same average Jacobi constant. To construct an initial guess for a torus, a perturbation of $\epsilon = 5 \times 10^{-5}$ in Eq. 4 is used to step along an eigenvector associated with the oscillatory mode. Then, each torus is computed using $N_Q = 25$ states along each of the $M_Q + 1 = 4$ invariant curves. Using the torus computation method presented by Jorba, Gómez and Mondelo, and Olikara and Scheeres, 20 invariant tori are computed along the family near each resonance [13–15]; note that the 20th torus lies at the boundary of the range of tori that are computed with the selected invariant curve discretization, but additional tori may exist further along the family. Invariant tori in each family that possess the largest out-of-plane displacement at apolune are displayed at the boundaries of Fig. 2 with a color scheme that is consistent with the periodic orbits in the center of the figure.

Point solutions for natural transfers are constructed to flow away from the torus near the 3:2 resonance that is displayed on the left of Fig. 2 and flow into the 1:2 resonance on the right of this figure. The unstable manifold of

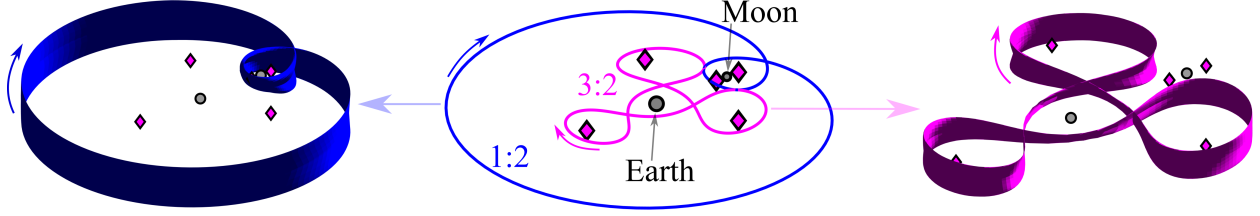


Fig. 2 Sample invariant tori and generating periodic orbits in the Earth-Moon CR3BP at $C_J = 2.73$ in the 1:2 (blue) and 3:2 (magenta) resonant orbit families.

the torus near the 3:2 resonance and the stable manifold of the torus near the 1:2 resonance are both generated using invariant curves at 101 values of θ_1 , i.e., in the longitudinal direction along each torus. These manifolds are propagated for up to 12 returns to the $y = 0$ surface of section, in any direction; recall that the first 6 map crossings for each trajectory are excluded from this analysis as they tend to remain close to the generating torus. The remaining intersections of the manifolds with the surface of section produce a total of 15,114 and 14,925 crossings for the 3:2 and the 1:2 resonances, respectively. Figure 3a displays the intersections of the generated subset of the invariant manifolds with the $y = 0$ surface of section via a projection onto the (x, \dot{x}) plane. In this projection, the intersections associated with the tori resemble the crossings of the stable and unstable manifolds associated with the planar periodic orbits in Fig. 1a). However, the increased complexity of these five-dimensional map crossings becomes apparent in a three-dimensional projection onto the (x, \dot{x}, z) space, as depicted in Fig. 3b): the crossings of these manifold arcs possess a significant out-of-plane component. Both the two- and three-dimensional representations displayed in Fig. 3a-b) do not completely represent the higher-dimensional intersections of the invariant manifolds with the surface of section. Thus, two map crossings that are located nearby in either of these two- or three-dimensional projections may not be close in the full five-dimensional phase space. Including a fourth dimension or introducing further constraints in the problem could mitigate this problem. However, including a fourth dimension would further complicate the visualization and analysis of the Poincaré map, while the design space may significantly shrink with additional constraints.

UMAP is employed to reduce the complexity of visualizing the large set of five-dimensional data via a projection onto a two-dimensional Euclidean space. The map crossings associated with both the stable and unstable manifolds are combined to form the complete dataset that is input to UMAP. Using the selected input parameters, UMAP produces the projection onto a two-dimensional space that is displayed in the center of Fig. 4. In this figure, the blue markers indicate map crossings of the stable manifold associated with the torus near the 1:2 resonance, while the magenta markers correspond to the unstable manifold associated with the torus near the 3:2 resonance. The two axes, labeled U_1 and U_2 , correspond to two variables that define the two-dimensional space calculated by UMAP. The projection calculated by UMAP minimizes the differences between the fuzzy topological structure of the original higher-dimensional data and the lower-dimensional representation. As a result, two map crossings that are close in the full phase space are expected to be located nearby in the two-dimensional projection. Analysis of this projection at the center of Fig. 4 reveals that

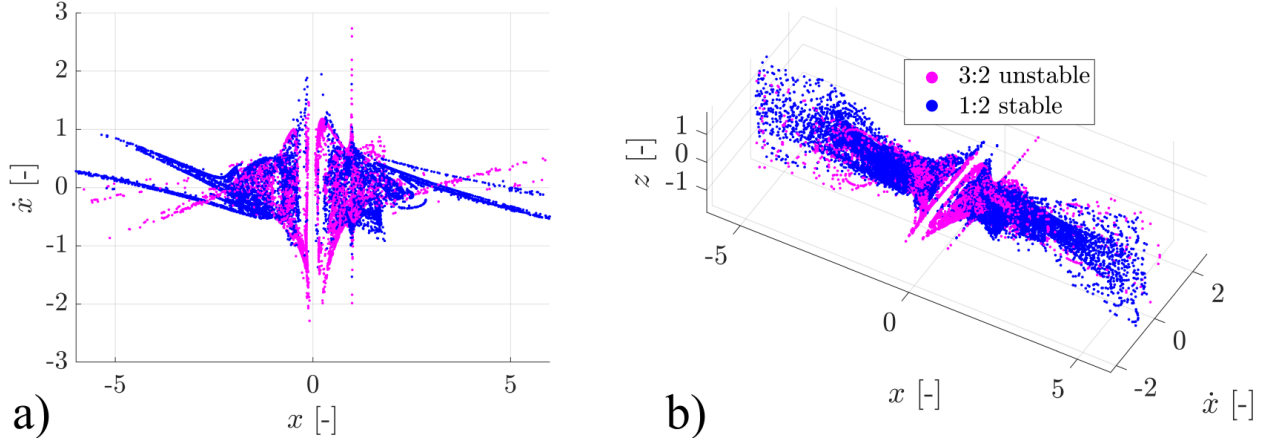


Fig. 3 Projections of the intersections of the hyperbolic manifolds from tori near the 1:2 (blue) and 3:2 (magenta) resonances with the $y = 0$ plane.

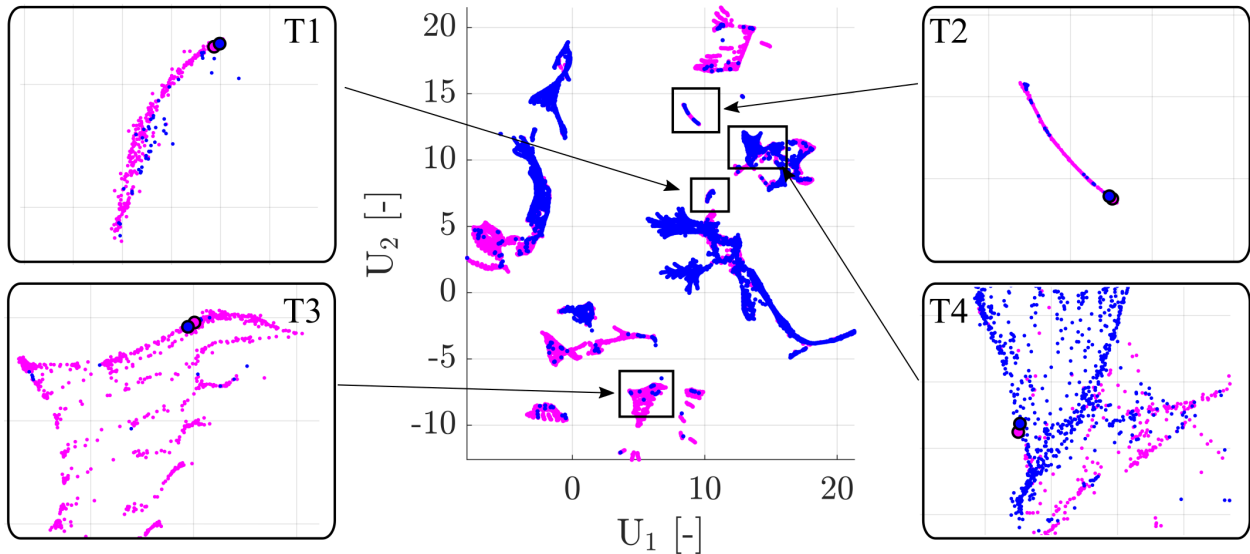


Fig. 4 Center: two-dimensional embedding of the map crossings in Fig. 3 from UMAP. Boundaries: zoomed-in views of four regions of interest.

there are multiple regions of both blue and magenta markers where the stable and unstable manifolds may potentially cross the $y = 0$ surface of section with similar state vectors: these regions are used to identify suitable map crossings to generate an initial guess for a nearby continuous transfer between the two tori. Four interesting regions appear in the zoomed-in plots at the boundaries of Fig. 4 and are used to generate four distinct transfers.

Identifying map crossings that are used to form initial guesses by analyzing this two-dimensional embedding reduces the complexity of analysis and computation. For instance, a specific region of the embedding captures a subset of the entire dataset of manifold crossings. These regions may be directly searched to locate nearby crossings from each set that possess a low relative distance in the two-dimensional projection. This approach reduces the number of computed pairwise distances in a brute-force search and the number of state components processed in each pairwise distance

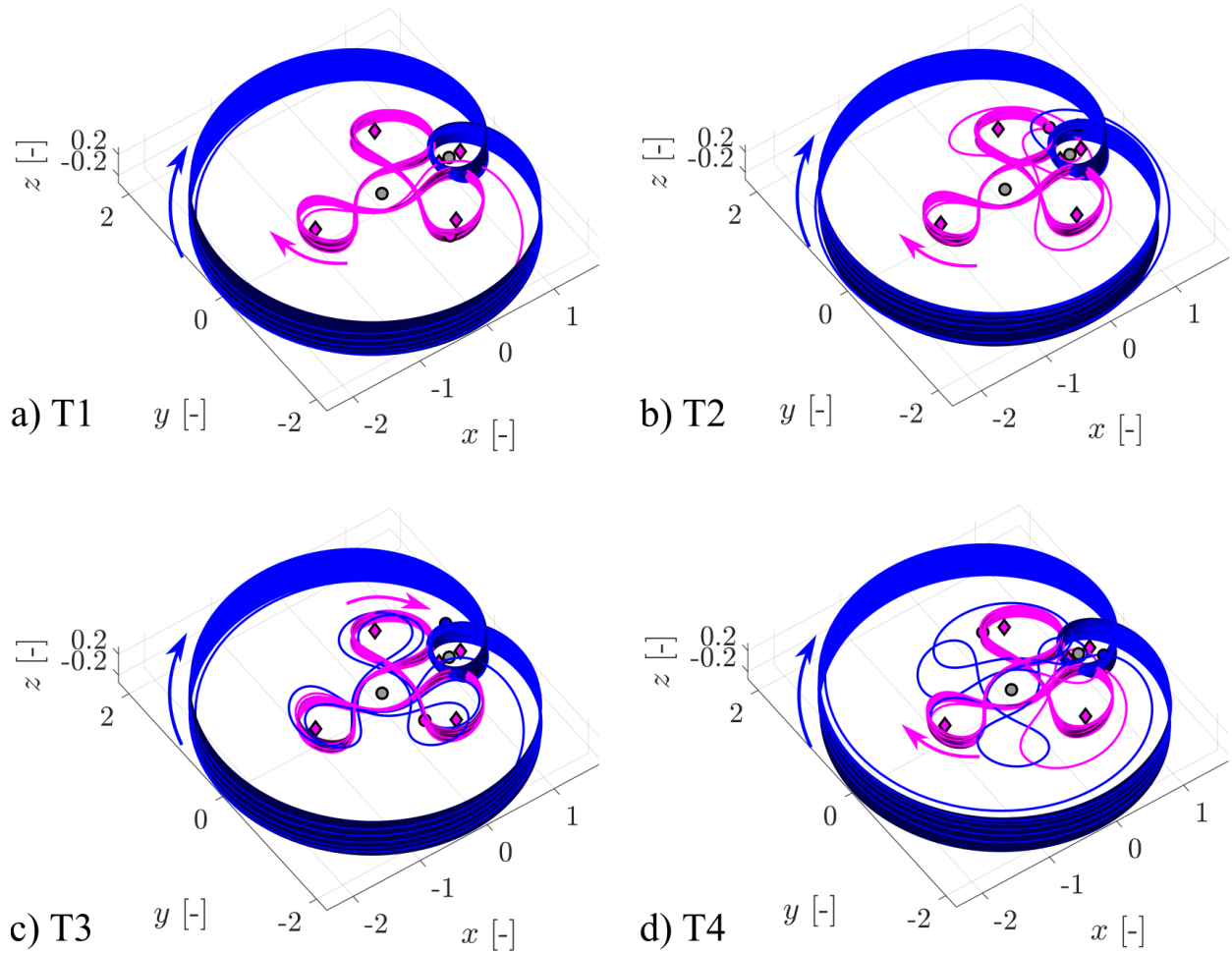


Fig. 5 Selected natural transfers from tori near the 3:2 to tori near the 1:2 resonances, labeled by the region in Fig. 4.

computation. More importantly, this two-dimensional visualization is also straightforwardly examined by a human to narrow down suitable regions where nearby map crossings may lie.

Each of the four regions of nearby map crossings on the two-dimensional projection calculated by UMAP is used to generate point solutions for a natural transition between invariant tori associated with the 3:2 and 1:2 resonances in the Earth-Moon CR3BP. Within each of the zoomed-in regions displayed at the boundaries of Fig. 4 map crossings that exist nearby on the projected space are selected from each of the unstable manifold associated with the invariant torus near the 3:2 resonance and the stable manifold associated with the invariant torus near the 1:2 resonance. The process described in the previous section produces four discontinuous initial guesses that are then used to recover the natural transfers that are displayed in Fig. 5 and labeled as T1-T4, consistent with the zoomed-in view in Fig. 4. Each of the depicted transfers is recovered in a computational time of approximately 15 seconds per trajectory on a computer with an i7-2600K 3.40GHz processor while remaining close to the initial guess. In Fig. 5 the selected transfers begin near

the magenta circle marker on the torus associated with the 3:2 resonant orbit family and terminate near the blue circle marker on the torus associated with the 1:2 resonant orbit family. Segments of each continuous trajectory are colored in magenta (or blue) according to the portion of the initial guess that was selected from the unstable (or stable) manifold. These four natural transfers between the selected invariant tori exhibit distinct geometries due to the specific manifold arcs used to construct the initial guess.

The intersections of the computed trajectories with the surface of section at $y = 0$ are highlighted in the traditional Poincaré map projections onto the (x, \dot{x}) plane, and the (x, \dot{x}, z) space in Fig. 6(a-b), respectively. The general set of intersections of the 3:2 unstable manifold (magenta) and the 1:2 stable manifold (blue) with the surface of section, as depicted previously in Fig. 3 are displayed with semi-transparent markers, while the intersections of the T1 to T4 transfers with the surface of section appear as gray circles. The map crossings of the T1 to T4 transfers appear to be located near potential intersections of the projections of the stable and unstable manifold map crossings onto a subset of the phase space. However, locating these intersections in the full five-dimensional dataset may have been particularly challenging using existing techniques.

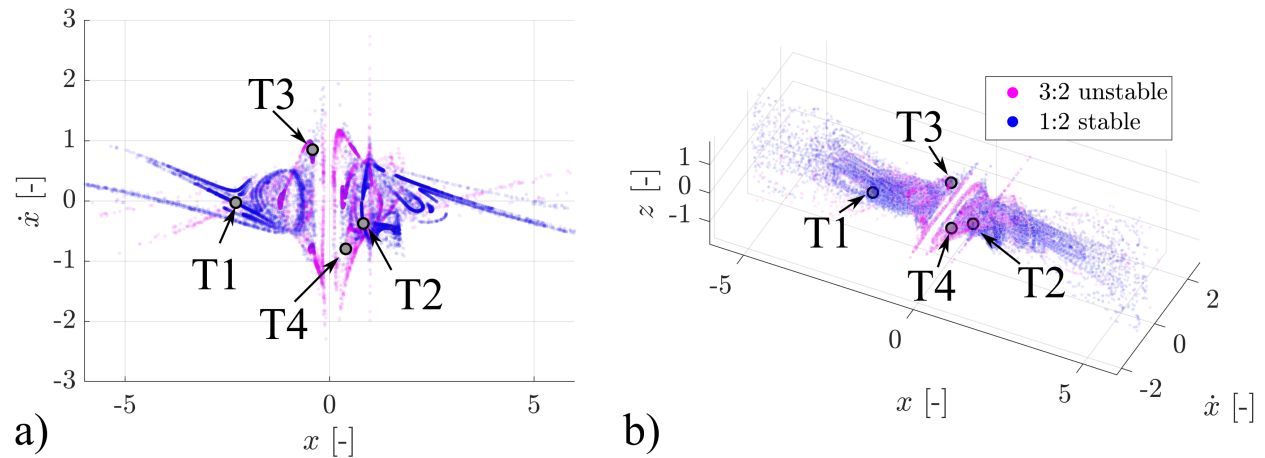


Fig. 6 Locating intersections of the corrected transfers with $y = 0$ on a map capturing the manifold crossings for tori near the 1:2 (blue) and 3:2 (magenta) resonances.

Additional natural transfers may possess map crossings that lie close to those of the computed transfers in the two-dimensional projection constructed by UMAP. Consider, for example, further examination of the zoomed-in area labeled as T2 in Fig. 4 and displayed with a higher resolution at the center of Fig. 7. Note that the complete embedding constructed by UMAP is also displayed in the bottom-left corner of the central figure to indicate the location of the selected region. Within the collection of projected map crossings in the center of Fig. 7 four pairs of map crossings are highlighted with blue and magenta circles. These pairs are selected to possess a low relative pairwise distance in the projected space. Each selected pair is then used to construct a discontinuous initial guess and corrected to generate a continuous natural transfer between the selected tori in the 3:2 and 1:2 resonant orbit families. The generated

transfers are displayed in the configuration space at the boundaries of Fig. 7 with projections onto the xy -, xz -, and yz -planes depicted in gray. Arrows are used to associate each transfer to the corresponding pair of map crossings in the two-dimensional projection. The transfers on the left of Fig. 7 possess a similar geometry to each other, with only minor differences in the apogee locations. The transfers on the right of this figure, however, possess a similar geometry to each other, but not to the transfers on the left. These results demonstrate both the vast solution space of the existing natural transfers between the selected 2-tori as well as the potential for families of transfers with similar geometries but distinct arrival and departure conditions to span regions of the two-dimensional projection. Further examining the existence and geometry of the broader array of transfers that are rapidly identified using the projection constructed by UMAP is an avenue of future work.

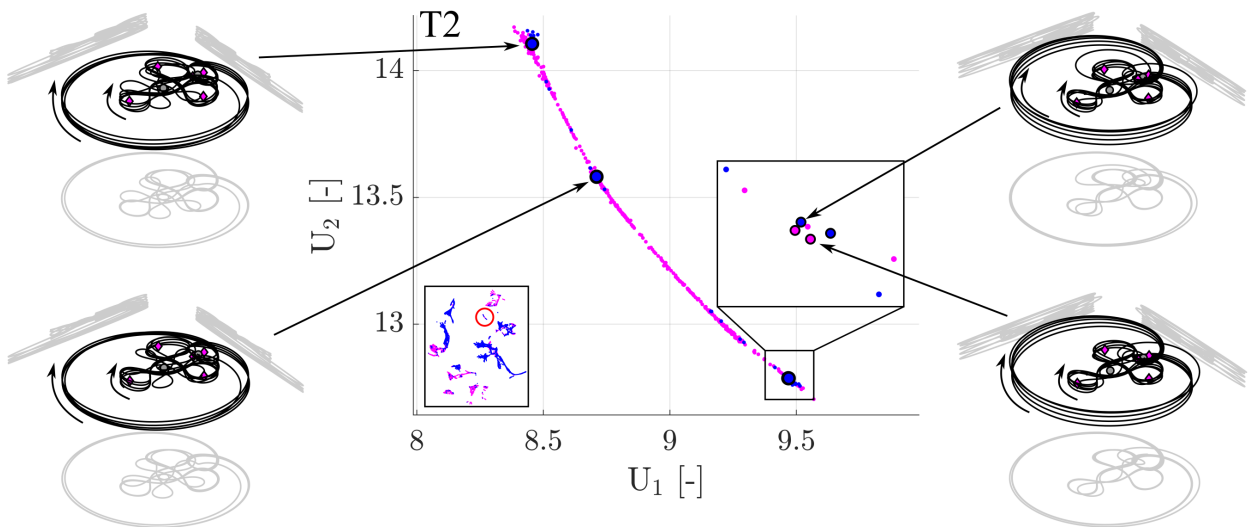


Fig. 7 Center: specific regions of the projected map crossings, labeled as T2 in Fig. 4. Boundaries: natural transfers constructed using selected map crossings pairs.

B. Family continuation

Continuation is used to generate natural transfers with similar geometries to transfer T1, plotted in Fig. 5a), but connecting additional members of the two families of invariant tori near the 3:2 and 1:2 resonances at $C_J = 2.73$. Note, however, that continuation is not used to find similar transfers connecting the tori at various longitudinal and transverse angles; rather, only a single transfer between two tori is sought. Fig. 8 displays a summary of the computed natural transfers for this particular transfer geometry from tori near the 3:2 resonance to tori near the 1:2 resonance. In the top-right plot of this figure, the horizontal and vertical axes depict the maximum out-of-plane component of the position vector at apogee along the departure and arrival tori, respectively. Each black marker in this two-dimensional representation indicates that a feasible natural transfer is computed to solve the optimization problem summarized in Eq. 7 with $f(\mathbf{V}) < 10^{-12}$ and $\|\mathbf{F}(\mathbf{V})\|_2 < 10^{-12}$. Four sample transfers, labeled as A1 to A4 and connecting the indicated

tori, are also displayed at the boundaries of the figure. Within these subfigures, the Earth and the Moon appear as gray circles, and the Earth-Moon Lagrange points are plotted as magenta diamonds.

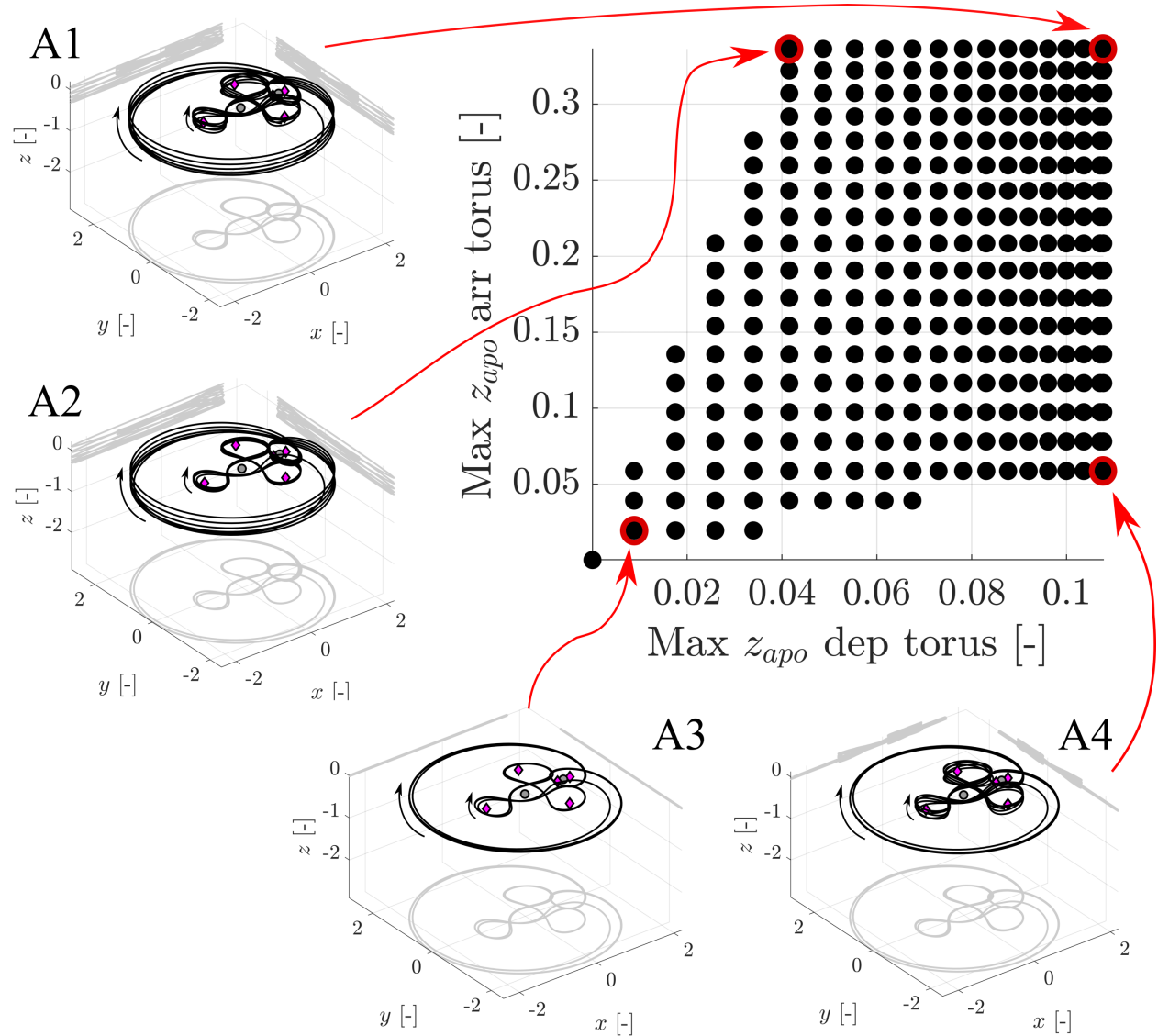


Fig. 8 Existence of natural transfers with a similar geometry to T1 between tori in the 3:2 and 1:2 resonances; sample transfers indicated in the boundaries.

Across the generated family of natural transfers from tori in the 3:2 resonant orbit family to tori in the 1:2 resonant orbit family, the solutions admit a similar geometry. However, as observed in the gray lateral xz - and yz -projections at the boundaries of Fig. 8 each transfer connects invariant tori with distinct out-of-plane displacements. For example, transfer A1 connects the 20th computed members of the families of invariant tori near the 3:2 and 1:2 resonances, which admit the largest out-of-plane displacement. Transfer A1 also exhibits the largest out-of-plane motion of the transfers computed. Conversely, transfer A3 connects the second computed tori in each of these two families, and the transfer is almost planar. Transfer A2 starts from an almost planar torus in the 3:2 resonant orbit family and approaches the 20th

computed member of the arrival torus in the 1:2 resonant orbit family. Transfer A4 exhibits an initially relatively large out-of-plane displacement, culminating with almost planar motion.

Analysis of Fig. 8 reveals useful insights into the existence of natural transitions between tori within each family. Specifically, given a fixed initial torus near the 3:2 resonance, a transition only exists to selected quasi-periodic trajectories near the 1:2 resonance and vice versa. The existence of these transitions, for this particular transfer geometry, appears to be linked to the relative difference in the maximum out-of-plane component along each torus. For initial tori near the 3:2 resonance with a small out-of-plane deviation, only tori near the 1:2 resonance with a small out-of-plane component are naturally accessible in the CR3BP. As the tori evolve along each family, natural transitions occur at a larger range of differences in the maximum out-of-plane components.

A similar continuation approach is used to generate natural transfers with similar geometries to transfer T4, plotted in Fig. 5a), that connect additional members of the two families of invariant tori near the 3:2 and 1:2 resonances at $C_J = 2.73$. This point solution, T4, naturally connects the 20th computed members of each of the selected families of invariant tori. However, there is an evident geometric difference between transfer T1 and T4: the transfer labeled as T4 exhibits a transient phase with multiple revolutions in the Earth vicinity prior to a final flyby with the Moon that directs the spacecraft towards a natural approach into the torus near the 1:2 resonance; of the four transfers in 5a), T4 deviates most significantly from the initial and final tori. The associated set of transfers computed via continuation from T4 are summarized in Fig. 9 using a configuration consistent with Fig. 8. Analysis of Fig. 9 reveals that this family of transfers resembling T4 encompasses a wider array of combinations of initial and final tori in the two families than transfers resembling T1. In fact, these natural transfers connect tori with relative large differences in the out-of-plane displacement. Such a result is likely due to the multiple close flybys performed by transfer T4 but not by transfer T1, as evident in Fig. 5a, d). Accordingly, the existence of natural transitions between spatial invariant tori in two distinct resonant orbit families appears to be influenced by the transfer geometry.

C. Recovering Transfers between Invariant Tori near Additional Resonances

The approach used to compute natural transfers between two invariant tori in the Earth-Moon CR3BP also supports constructing natural connections between tori near additional resonances. Consider, for example, designing a transfer from a torus near an orbit in the 3:1 resonant orbit family to a torus in the 1:3 resonant orbit family; both tori exist at $C_J = 3$. These two tori are computed with $N_Q = 25$ and $M_Q = 101$. Then, the intersections of each of the unstable and stable manifolds of the initial and final torus, respectively, with the $y = 0$ plane, are computed for up to 18 returns; only the last 8 crossings deviate significantly from the initial and final tori and are, therefore, examined further. These crossings of the unstable and stable manifolds of the initial and final torus are projected onto a two-dimensional space that is computed by UMAP. This projection is displayed in Fig. 10a): the crossings of the unstable manifold of a torus near the 3:1 resonant family appear in magenta whereas the crossings of the stable manifold arcs approaching

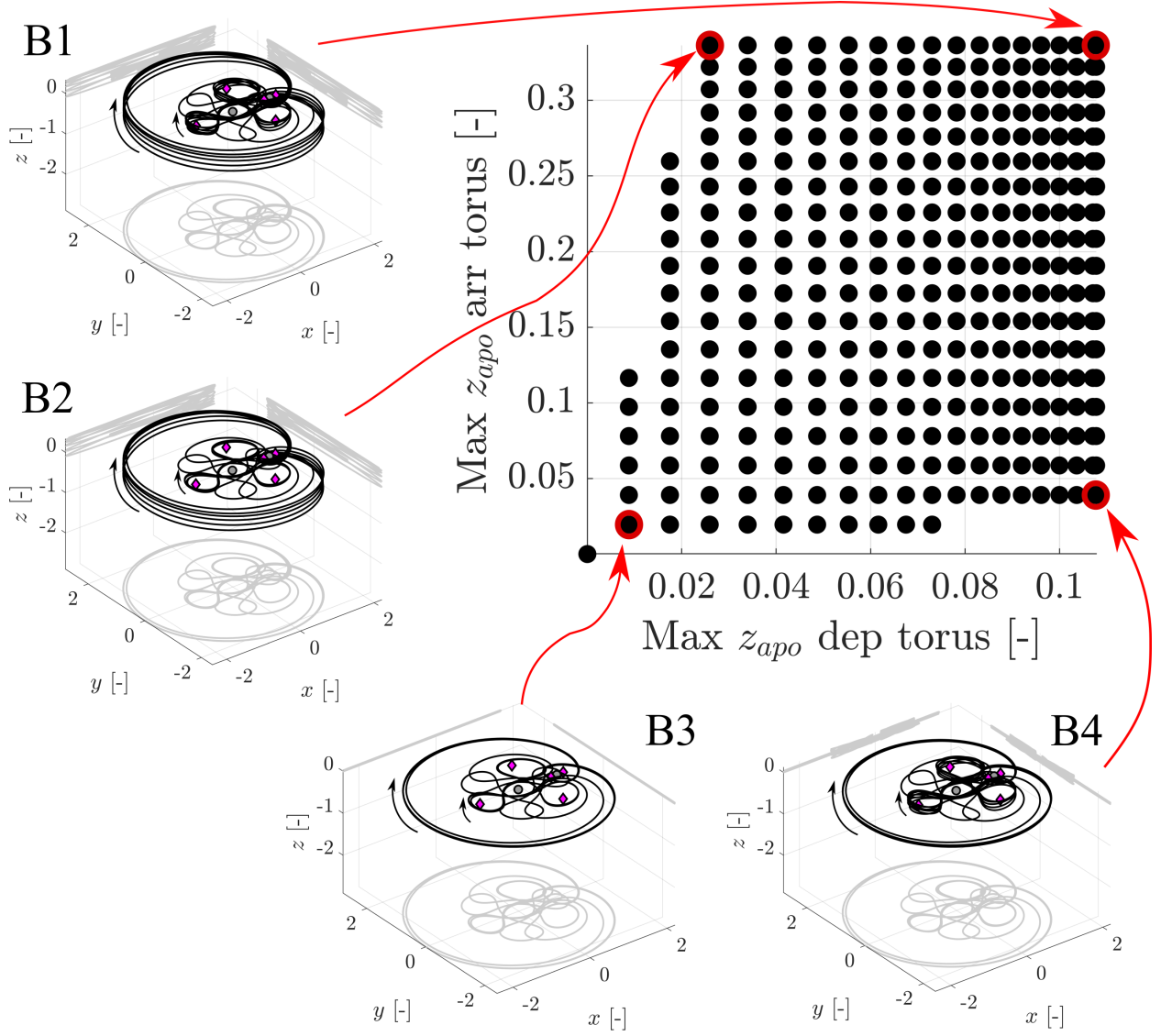


Fig. 9 Existence of natural transfers with a similar geometry to T4 between tori in the 3:2 and 1:2 resonances; sample transfers indicated in the boundaries.

a torus near the 1:3 resonance are displayed in blue. To construct an initial guess for a natural transfer departing the torus near the 3:1 resonance and naturally approaching the torus near the 1:3 resonance, the framed region from the UMAP projection in Fig. 10a) is investigated. In this region, a projected map crossing is selected from each of the stable and unstable manifold sets to possess the smallest relative distance. The resulting discontinuous initial guess is corrected and visualized in the configuration space in Fig. 10b), using a coloring scheme consistent with Fig. 5. Figure 11 displays similar information for transfers departing from a torus near the 2:3 resonance and approaching a torus near the 1:5 resonance in the Earth-Moon CR3BP at $C_J = 2.6$. Of course, these transfers that are visualized in Figs. 10 and 11 are simply point solutions among a variety of natural transfers that may be identified through the presented approach. In fact, additional transfers with distinct geometries may be generated by investigating other regions of the

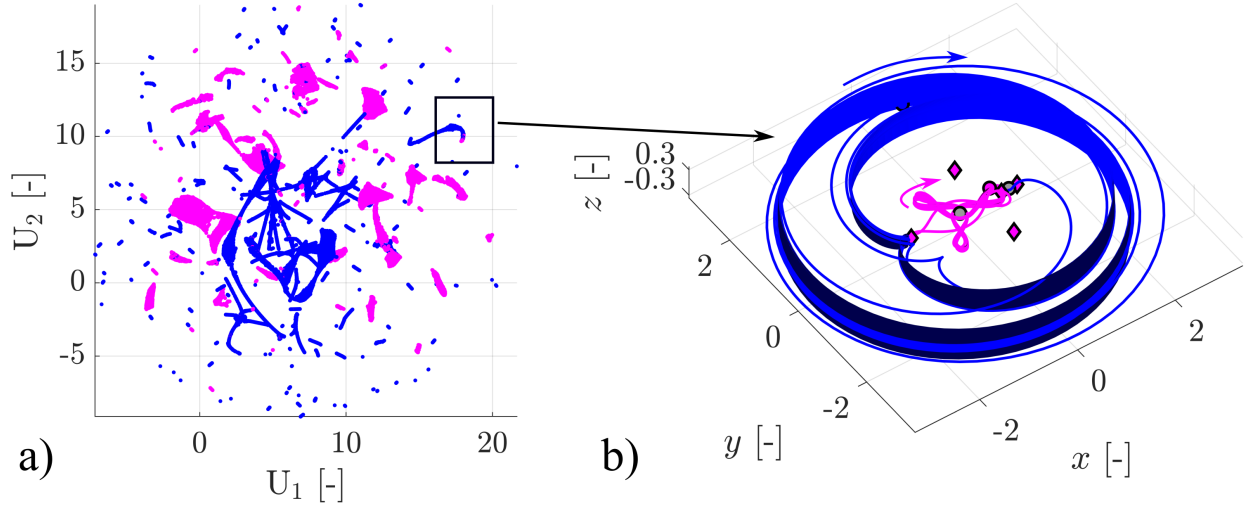


Fig. 10 a) Embedding of the map crossings of the hyperbolic manifolds of invariant tori near the 1:3 (blue) and the 3:1 (magenta) resonances; b) constructed natural transfer.

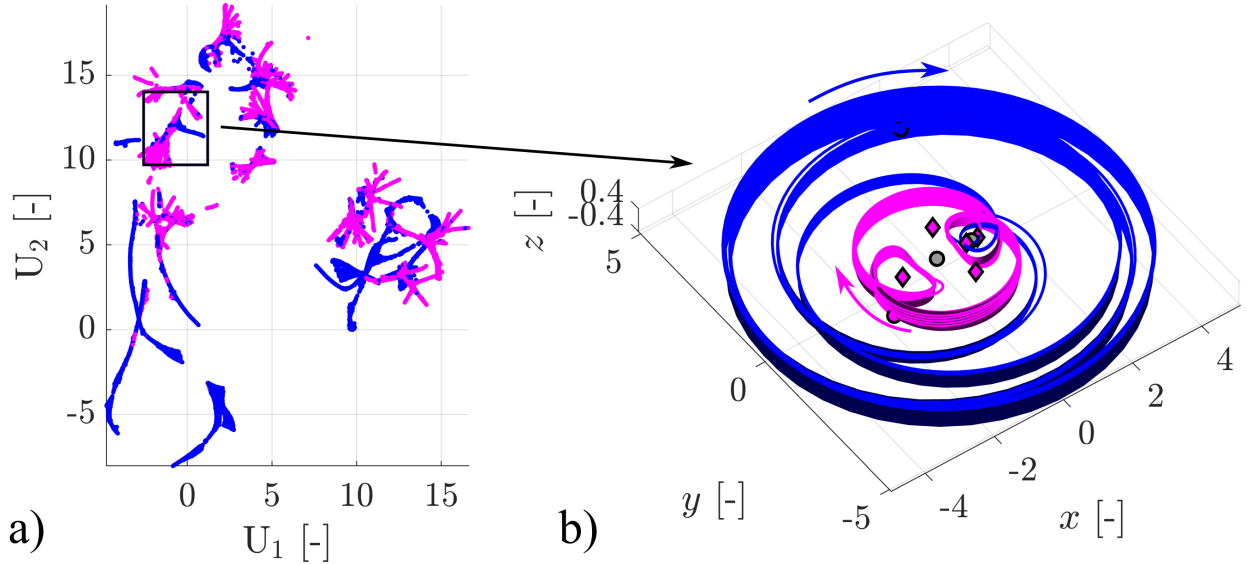


Fig. 11 a) Embedding of the map crossings of the hyperbolic manifolds of invariant tori near the 1:5 (blue) and the 2:3 (magenta) resonances; b) constructed natural transfer.

projected spaces in Figs. 10a) and 11a), as well as different combinations of map crossings in the same framed areas. However, these two examples demonstrate the capability to use the presented approach to recover a wider variety of natural transfers between tori near resonant orbit families in the Earth-Moon CR3BP.

VIII. Conclusions

Natural transitions between 2-tori near mean-motion resonances in the CR3BP can be computed numerically from an initial guess that is constructed via a combination of dynamical systems theory and dimension reduction.

Specifically, intersections of the stable and unstable manifolds of distinct 2-tori can be summarized by their crossings with a surface of section. Although these crossings possess a higher-dimensional description, they can be visualized in a lower-dimensional space that is computed using manifold learning, a form of nonlinear dimension reduction. This lower-dimensional representation can guide the identification of candidate arcs along each hyperbolic invariant manifold that form a useful initial guess for a natural connection between distinct 2-tori. This approach leads to the successful computation of natural connections of various geometries between a variety of invariant 2-tori near the 3:1 and 1:3 resonances, and near the 1:5 and the 2:3 resonances, in the Earth-Moon CR3BP.

IX. Acknowledgments

An earlier version of this paper was presented as paper AAS 20-724 at the AAS/AIAA Astrodynamics Specialist Conference in August 2020. The work in this paper also appears in the first author's Ph.D. dissertation titled "Incorporating Machine Learning into Trajectory Design Strategies in Multi-Body Systems", submitted in April 2022 to the University of Colorado Boulder. The authors also thank the reviewers for their feedback.

References

- [1] Bonasera, S., "Incorporating Machine Learning into Trajectory Design Strategies in Multi-Body Systems," Ph.D. thesis, Ann and H.J. Smead Aerospace Engineering Sciences, University of Colorado Boulder, Boulder, CO, 2022.
- [2] Carrico, J. Jr., Dichmann, D., Policastri, L., Carrico, J. III, Craychee, T., Ferreira, J., Intelisano, M., Lebois, R., Loucks, M., Schrifft, T., and Sherman, R., "Lunar-Resonant Trajectory Design for the Interstellar Boundary Explorer (IBEX) Extended Mission," *Advances in the Astronautical Sciences*, Vol. 142, December 2011, pp. 771 – 789.
- [3] Dichmann, D., Parker, J., Nickel, C., and Lutz, S., "Trajectory Design for the Transiting Exoplanet Survey Satellite," *International Symposium on Spacecraft Flight Dynamics*, Laurel, MD, May 2014.
- [4] Short, C., Howell, K.C., Haapala, A., and Dichmann, D., "Mode Analysis for Long-Term Behavior in a Resonant Earth-Moon Trajectory," *Journal of the Astronautical Sciences*, Vol. 64, 2017, pp. 156 – 187. <https://doi.org/10.1007/s40295-016-0098-9>
- [5] Anderson, R.L., "Tour Design Using Resonant-Orbit Invariant Manifolds in Patched Circular Restricted Three-Body Problems," *Journal of Guidance, Control, and Dynamics*, Vol. 44, No. 1, January 2021, pp. 106–119. <https://doi.org/10.2514/1.G004999>
- [6] Anderson, R.L.; Lo, M.W., "Role of Invariant Manifolds in Low-Thrust Trajectory Design," *Journal of Guidance, Control, and Dynamics*, Vol. 32, No. 6, November-December 2009, pp. 1921–1930. <https://doi.org/10.2514/1.37516>
- [7] Koon, W.S., Lo, M.W., Marsden, J.E., and Ross, S.D., "Resonance and Capture of Jupiter Comets," *Celestial Mechanics and Dynamical Astronomy*, Vol. 81, No. 27, September 2001, pp. 27 – 38. <https://doi.org/10.1023/A:1013398801813>

- [8] Barrabés, E., Mondelo, M.J., and Ollé, M., “Numerical continuation of families of heteroclinic connections between periodic orbits in a Hamiltonian system,” *Nonlinearity* 26 2747, Vol. 26, No. 10, 2013, pp. 2747–2765. <https://doi.org/10.1088/0951-7715/26/10/2747>
- [9] Duarte, G., and Jorba, À., “Using normal forms to study Oterma’s transition in the Planar RTBP,” *Discrete and Continuous Dynamical Systems - B*, Vol. 28(1), 2023, pp. 230–244. <https://doi.org/10.3934/dcdsb.2022073>
- [10] Lykawka, P.S., and Mukaia, T., “Resonance sticking in the scattered disk,” *Icarus*, Vol. 192, 2017, pp. 238 – 247. <https://doi.org/10.1016/j.icarus.2007.06.007>
- [11] Haapala, A.F., and Howell, K.C., “Trajectory Design Strategies Applied to Temporary Comet Capture Including Poincaré Maps and Invariant Manifolds,” *Celestial Mechanics and Dynamical Astronomy*, Vol. 116, 2013, pp. 299 – 323. <https://doi.org/10.1007/s10569-013-9490-y>
- [12] Calleja, R. C., Doedel, E. J., Humphries, A. R., Lemus, A., and Oldeman, B. E., “Boundary-Value Problem Formulations for Computing Invariant Manifolds and Connecting Orbits in the Circular Restricted Three Body Problem,” *Celestial Mechanics and Dynamical Astronomy*, Vol. 114, 2012, pp. 77–106. <https://doi.org/10.1007/s10569-012-9434-y>
- [13] Jorba, À., “Numerical Computation of the Normal Behavior of Invariant Curves of n-Dimensional Maps,” *Nonlinearity*, Vol. 14, No. 5, 2001, pp. 943 – 976. <https://doi.org/10.1088/0951-7715/14/5/303>
- [14] Gómez, G., and Mondelo, J.M., “The Dynamics Around the Collinear Equilibrium Points of the RTBP,” *Physica D*, Vol. 157, No. 4, 2001, pp. 283 – 321. [https://doi.org/10.1016/S0167-2789\(01\)00312-8](https://doi.org/10.1016/S0167-2789(01)00312-8)
- [15] Olikara, Z.P., and Scheeres, D.J., “Numerical Method for Computing Quasi-Periodic Orbits and their Stability in the Restricted Three-Body Problem,” *IAA Conference on Dynamics and Control of Space Systems*, Porto, Portugal, March 2012.
- [16] Olikara, Z., “Computation of Quasi-Periodic Tori and Heteroclinic Connections in Astrodynamics Using Collocation Techniques,” Ph.D. thesis, Ann and H.J. Smead Aerospace Engineering Sciences, University of Colorado Boulder, Boulder, CO, 2016.
- [17] McCarthy, B., “Cislunar Trajectory Design Methodologies Incorporating Quasi-Periodic Structures with Applications,” Ph.D. thesis, School of Aeronautics & Astronautics, Purdue University, West Lafayette, IN, 2022.
- [18] Kumar, B., Anderson, R. L., and de la Llave, R., “Using GPUs and the parameterization method for rapid search and refinement of connections between tori in periodically perturbed planar circular restricted 3-body problems,” *Proceedings of the 2021 AAS/AIAA Space Flight Mechanics Meeting*, Vol. 176, 2021, pp. 2311–2330.
- [19] Murphy, K.P., *Probabilistic Machine Learning: An Introduction*, MIT Press, 2022, Chap. 20. URL probml.ai
- [20] McInnes, L., Healy, J., and Melville, J., “UMAP: Uniform Manifold Approximation and Projection for Dimension Reduction,” *ArXiv e-prints*, February, 2018. ArXiv: 1802.03426.

- [21] Cao, J., Spielmann, M., Qiu, X., Huang, X., Ibrahim, D.M., Hill, A.J., Zhang, F., Mundlos, S., Christiansen, L., Steemers, F.J., Trapnell, C., and Shendure, J., “The Single-Cell Transcriptional Landscape of Mammalian Organogenesis,” *Nature*, Vol. 566, 2019, pp. 496 – 502. <https://doi.org/10.1038/s41586-019-0969-x>
- [22] Diaz-Papkovich, A., Anderson-Trocme, L., Ben-Eghan, C., and Gravel, S., “UMAP Reveals Cryptic Population Structure and Phenotype Heterogeneity in Large Genomic Cohorts,” *PLoS Genetics*, Vol. 15, No. 11, 2019. <https://doi.org/10.1371/journal.pgen.1008432>
- [23] Bloch, T., Watt, C., Owens, M., McInnes, L., and Macneil, A.R., “Data-Driven Classification of Coronal Hole and Streamer Belt Solar Wind,” *Solar Physics*, Vol. 295, No. 41, 2020. <https://doi.org/10.1007/s11207-020-01609-z>
- [24] Szebehely, V., *Theory of Orbits: The Restricted Problem of Three Bodies*, Academic Press, London, UK, 1967, Chaps. 1, 5.
- [25] Vaquero, M., “Spacecraft Transfer Trajectory Design Exploiting Resonant Orbits in Multi-Body Environments,” Ph.D. thesis, School of Aeronautics & Astronautics, Purdue University, West Lafayette, IN, 2013.
- [26] Anderson, R.L., and Lo, M.W., “Dynamical Systems Analysis of Planetary Flybys and Approach: Planar Europa Orbiter,” *Journal of Guidance, Control, and Dynamics*, Vol. 33, No. 6, 2010. <https://doi.org/10.2514/1.45060>
- [27] Barrabés, E., and Gómez, G., “Spatial p-q Resonant Orbits of the RTBP,” *Celestial Mechanics and Dynamical Astronomy*, Vol. 84, 2002, p. 387 – 407. <https://doi.org/10.1023/A:1021137127909>
- [28] Koon, W., Lo, M., Marsden, J., and Ross, S., *Dynamical Systems, the Three-Body Problem and Space Mission Design*, Marsden Books, 2011, Ch. 4.
- [29] Verhulst, F., *Nonlinear Differential Equations and Dynamical Systems*, Springer-Verlag, Berlin, Heidelberg, 1996, Chap. 5. <https://doi.org/10.1007/978-3-642-61453-8>
- [30] Haapala, A., “Trajectory Design in the Spatial Circular Restricted Three-Body Problem Exploiting Higher-Dimensional Poincaré Maps,” Ph.D. thesis, School of Aeronautics & Astronautics, Purdue University, West Lafayette, IN, 2014.
- [31] Baresi, N., “Spacecraft Formation Flight on Quasi-Periodic Invariant Tori,” Ph.D. thesis, Ann and H.J. Smead Aerospace Engineering Sciences, University of Colorado Boulder, Boulder, CO, 2017.
- [32] Perko, L., *Differential Equations and Dynamical Systems, 3rd Edition*, Springer, New York, 2000, Ch. 3.
- [33] Gómez, G., Koon, W.S., Lo, M.W., Marsden, J.E., Masdemont, J., and Ross, S.D., “Connecting Orbits and Invariant Manifolds in the Spatial Restricted Three-Body Problem,” *Nonlinearity*, Vol. 17, 2004, pp. 1571–1606. <https://doi.org/10.1088/0951-7715/17/5/002>
- [34] McInnes, L., Healy, J., and Astels, S., “How UMAP Works,” 2016. URL https://umap-learn.readthedocs.io/en/latest/how_umap_works.html accessed February 2022.

[35] M. Galassi, M., Davies, J., Theiler, J., Gough, B., Jungman, G., Alken, P., Booth, M., Rossi, F., and Ulerich, R., *GNU Scientific Library Reference Manual (3rd Ed.)*, ISBN 0954612078, 2021.

[36] MathWorks, "MATLAB," , 2021. Natick, MA, USA.